placed at a distance of 2 m and listeners could use four intervals (centred at 0, 1, 2 and 3 m) for their distance judgements. Because the low number of intervals could have affected the results (owing to the limited resolution and the possible occurrence of end effects), the interval number was doubled in the second experiment (intervals were now centred at 0–3.5 m in 0.5-m steps). In addition, the loudspeaker was moved to a distance of 3 m to check whether its position had introduced a bias. The 3-m gap was bridged by two poles, placed at distances of 1 and 2 m, that provided additional reference points. Six listeners participated in each experiment. A between-groups analysis of variance, applied to results of the two experiments, showed that the results for the conditions that were replicated did not differ significantly ($P = 0.73$). Thus, results were affected neither by the number of intervals nor by the position of the loudspeaker.

Received 3 December; accepted 21 December 1998.

1. Békésy, G. v. Über die Entstehung der Entfernungsempfindung beim Hören. *Akustische Z.* **3,** 21–31 (1938).
2. Mershon, D. H. & King, L. E. Intensity and reverberation as factors in the auditory perception of egocentric distance. *Percept. Psychophys.* **18,** 409–415 (1975).
3. Mershon, D. H. & Bowers, J. N. Absolute and relative cues for the auditory perception of egocentric distance. *Perception* **8,** 311–322 (1979).
4. Nielsen, S. H. Auditory distance perception in different rooms. *J. Audio Eng. Soc.* **41,** 755–770 (1993).
5. Wightman, F. L. & Kistler, D. J. Headphone simulation of free-field listening: II. Psychophysical validation. *J. Acoust. Soc. Am.* **85,** 868–878 (1989).
6. Bronkhorst, A. W. Localization of real and virtual sound sources. *J. Acoust. Soc. Am.* **98,** 2542–2553 (1995).
7. Houtgast, T. & Aoki, S. Stimulus-onset dominance in the perception of binaural information. *Hearing Res.* **72,** 29–36 (1994).
8. Coleman, P. D. Failure to localize the source distance of an unfamiliar sound. *J. Acoust. Soc. Am.* **34,** 345–346 (1962).
9. Coleman, P. D. An analysis of cues to auditory distance perception in free space. *Psychol. Bull.* **60,** 302–315 (1963).
10. Blauert, J. *Spatial Hearing* (MIT Press, Cambridge, Massachusetts, 1997).
11. Begault, D. R. Perceptual effects of synthetic reverberation on three-dimensional audio systems. *J. Audio Eng. Soc.* **40,** 895–904 (1992).
12. Moore, B. C. J., Glasberg, B. R., Plack, C. J. & Biswas, A. K. The shape of the ear's temporal window. *J. Acoust. Soc. Am.* **83,** 1102–1116 (1988).
13. Kuttruff, H. *Room Acoustics* (Applied Science, London, 1973).
14. Wettschureck, R., Plenge, G. & Lehringer, F. Entfernungswahrnehmung beim natürlichen Hören sowie bei kopfbezogenen Stereofonie. *Acustica* **29,** 260–272 (1973).
15. Møller, H., Sørensen, M. F., Hammershøi, D. & Jensen, C. B. Head-related transfer functions of human subjects. *J. Audio Eng. Soc.* **43,** 300–321 (1995).

Acknowledgements. Part of this research was done within the European AUDIS project.

Correspondence and requests for materials should be addressed to A.W.B. (e-mail: bronkhorst@tm.tno.nl)

The arrangement of the three cone classes in the living human eye

Austin Roorda*† & David R. Williams*

**Center for Visual Science, University of Rochester, Rochester, New York 14627, USA*

Human colour vision depends on three classes of receptor, the short- (S), medium- (M), and long- (L) wavelength-sensitive cones. These cone classes are interleaved in a single mosaic so that, at each point in the retina, only a single class of cone samples the retinal image. As a consequence, observers with normal trichromatic colour vision are necessarily colour blind on a local spatial scale[1]. The limits this places on vision depend on the relative numbers and arrangement of cones. Although the topography of human S cones is known[2,3], the human L- and M-cone submosaics have resisted analysis. Adaptive optics, a technique used to overcome blur in ground-based telescopes[4], can also overcome blur in the eye, allowing the sharpest images ever taken of the living retina[5]. Here we combine adaptive optics and retinal densitometry[6] to obtain what are, to our knowledge, the first images of the arrangement of S, M and L cones in the living human eye. The proportion of L to M cones is strikingly different in two male subjects, each of whom has normal colour vision. The mosaics of both subjects have large patches in which either M or L cones are missing. This arrangement reduces the eye's ability to recover colour variations of high spatial frequency in the environment but may improve the recovery of luminance variations of high spatial frequency.

We measured the eye's aberrations with a Hartmann–Shack wavefront sensor and compensated for them with a deformable mirror (see ref. 4 for details). We then collected images of the cone mosaic, as shown in Fig. 1a, with a charge-coupled device (CCD). Individual cones were classified by comparing images taken when the photopigments were fully bleached with those taken when the photopigments were either dark-adapted or exposed to a light that selectively bleached one photopigment. From these images, we created absorptance images that remove static features to reveal only the distribution of the photolabile pigments that distinguish the cone classes.

To distinguish S cones from M and L cones, we obtained absorptance images from dark-adapted and fully bleached images.

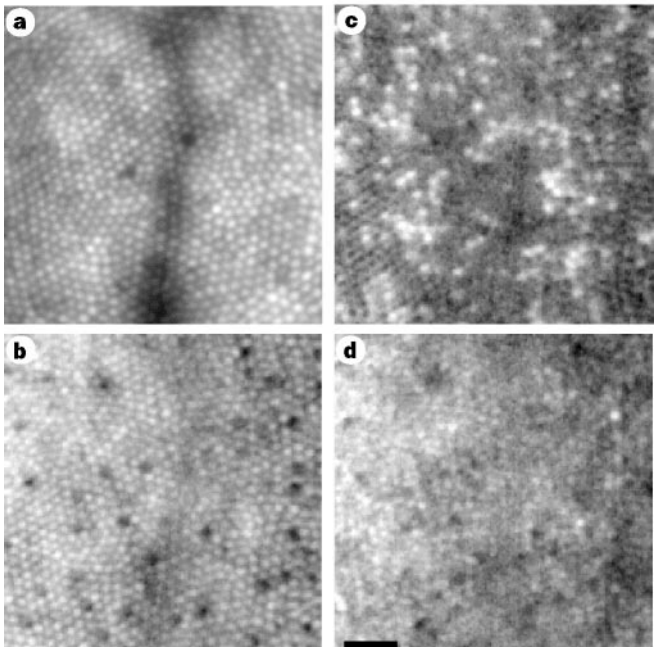

Figure 1 Images of the right eye of subject JW. The mosaic was illuminated with a 4-ms flash (1 degree diameter, ~0.3 μJ) through a 2-mm entrance pupil. Light of wavelength 550 nm was used to maximize absorptance by L- and M-cone photopigment. Images were obtained with a 6-mm exit pupil at a retinal eccentricity of one degree nasal from the foveal centre, which is located to the left of the image. For each retinal location, about 50 images taken over 5 days were averaged to increase the signal-to-noise ratio. Fixational eye movements translate the image from flash to flash, requiring registration with cross-correlation before averaging. **a,** A registered sum of 61 images taken after a full bleach. **b–d**, Absorptance images of the patch of cones shown in **a**, defined as 1 minus the ratio of the absorptance of a dark-adapted or selectively bleached image to the absorptance of the corresponding fully bleached image. Images of fully bleached retina were obtained following exposure to 550-nm light (70-nm bandwidth, 37×10^6 troland-seconds). Images of dark-adapted retina were taken following 5 min of dark adaptation. **b,** The absorptance image of dark-adapted cones, revealing a sparse array of S cones which appear dark because of their low absorptance at 550 nm. **c, d,** Absorptance images following a 470-nm (**c**) and 650-nm (**d**) selective bleach. Bleaching energies were set by calculation and then modified empirically to achieve the maximum possible difference between M- and L-photopigment concentration. The absorptance images for both bleaching conditions have higher pigment density toward the fovea; this is caused by the increases in the length of the outer segment and in macular pigment, which reduce bleaching in the 470-nm condition. Scale bar represents 5 arcmin of visual angle.

†Present address: University of Houston, College of Optometry, Houston, Texas 77204-6052, USA

Because S cones absorb negligibly at the imaging wavelength of 550 nm, whereas M and L cones absorb strongly at this wavelength, the S cones appear as a sparse array of dark cones in the absorptance image of Fig. 1b while the M and L cones appear bright. To distinguish L from M cones, we took images immediately after one of two bleaching conditions: dark-adapted retina was exposed to a 650-nm light, which selectively bleached the L pigment, or a 470-nm light, which selectively bleached the M pigment. The absorptance image for the 650-nm bleach reveals dark, low-absorptance L cones that have been heavily bleached and bright, highly absorbing M cones that were spared from bleaching (Fig. 1c). The absorptance image for the 470-nm bleach shows selective bleaching of M cones, but the effect is smaller than the effect of the 650-nm bleach because of the similarity of M-cone and L-cone action spectra at this wavelength (Fig. 1d).

Figure 2a–d shows that, for two trichromats with normal colour vision, the absorptances of single cones after 470-nm and 650-nm bleaches produce a bimodal distribution. If these modes represent L and M cones, then only a single mode should be observed in a similar experiment on a protanope, a person who lacks the L pigment. This prediction is confirmed by the data shown in Fig. 2e, f. Table 1 summarizes the numbers of S, M and L cones found in the two trichromats. The relative number of L and M cones differs greatly between these two subjects. In two patches of retina, one from the nasal and one from the temporal fovea, subject JW had a mean ratio of L to M cones of 3.79 whereas AN had a ratio of 1.15. This large individual difference is consistent with the variability found using psychophysical methods[7–10], spectral electroretinograms[11,12], microspectrophotometry[13,14] and messenger RNA analysis[15,16].

The arrangements of S, M and L cones for subjects JW and AN are shown in the psuedocolour images in Fig. 3. The distribution of the sparse S cones is not significantly different from random in either trichromat. This agrees with previous results[3] that showed that the developmental mechanism used to space S cones in a regular, nonrandom manner in humans is not seen near the fovea. Perhaps cone migration during the formation of the fovea disrupts regular S-cone spacing. The assignment of M and L cones is not significantly different from random in JW's eye but in AN's eye the M and L cones are significantly more aggregated than expected in a random mosaic. This additional clumping could arise if, for example, progenitor cells were to bias the 'decisions' of their progeny to express either M or L opsin. However, we cannot exclude the possibility that the departure from a random distribution in AN's eye is a consequence of residual optical blur in his retinal images. Optical blur could increase the chances of misclassifying especially those cones that are surrounded by cones of the opposite class, and this would exaggerate clumping. The overlap in the two distributions of Fig. 2d indicates that about 6% of AN's M and L cones were misidentified. Simulations suggest that this low error rate may nonetheless be high enough to produce the tendency towards the additional clumping we observed. Microspectrophotometry[17] on small foveal patches of excised talapoin retina indicated a random assignment of M and L cones and photopigment transmittance imaging in a macaque peripheral retina[18] showed a tendency towards aggregation of M and L cones. All studies agree that there is no tendency for the M cones to disperse themselves uniformly among the L cones, and the lack of a regular packing scheme for these cone classes may be ubiquitous among old-world primates.

What are the implications of this arrangement for vision? The coarse grain of the cone submosaics causes fluctuations in the

Table 1 Cone numbers for two subjects with normal colour vision

Subject	Number of cones	L cones (%)	M cones (%)	S cones (%)	Error (%)	L:M ratio
JW	1462	75.8	20.0	4.2	2.1	3.79
AN	522	50.6	44.2	5.2	5.6	1.15

The error column shows the percentage of cones labelled M (or L) that are actually L (or M) cones. The error in the assignment of L and M cones is taken to be the fractional area of the intersection of the sum of two gaussians used to fit the histograms shown in Fig. 2.

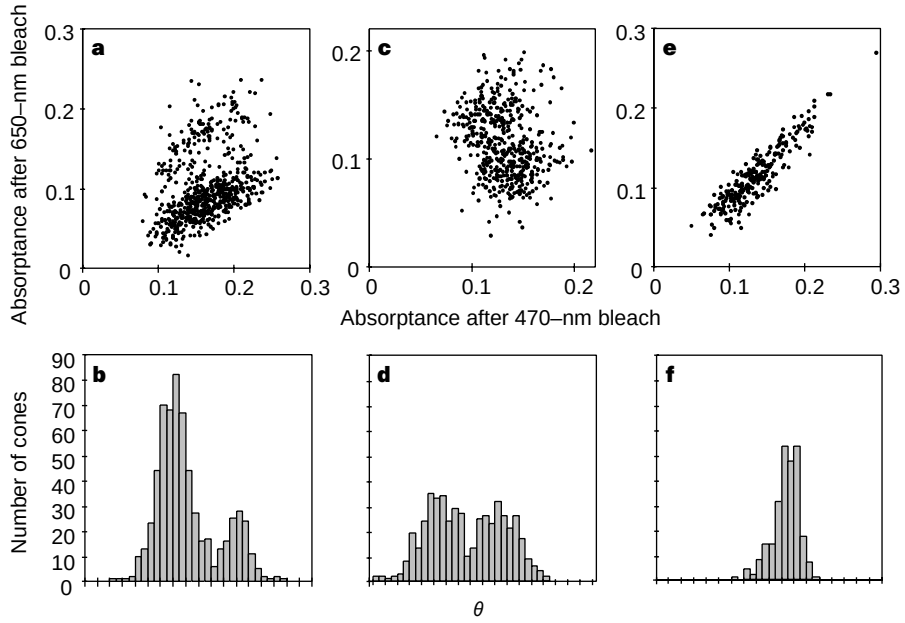

Figure 2 Scatter plots and histograms of individual cone absorptances. Scatter plots show the absorptance of each cone in a contiguous patch after the 470-nm and 650-nm selective bleaches. Cone absorptance was taken as the average value computed within a 0.4-arcmin square region centred on the cone. Histograms show the distribution of cones as a function of angle (θ) in the scatter plots. **a, b,** Results derived from the absorptance images of Fig. 1c, d, with S cones removed. **c, d,** Results obtained from a second trichromat, AN. For these trichromats, we fitted the sum of two gaussian curves to the histograms. The angle corresponding to the intersection of the two gaussian curves was used to categorize L and M cones. The fractional area of the overlap compared with the total area under the two gaussians provides an estimate of the fraction of cones that were misidentified; these estimates are 2.1% for JW and 5.6% for AN. **e, f,** Results obtained from a protanope whose colour deficiency was verified psychophysically and by genetic screening. As with the trichromats, bleaching levels were chosen to optimize the chance of distinguishing two pigments.

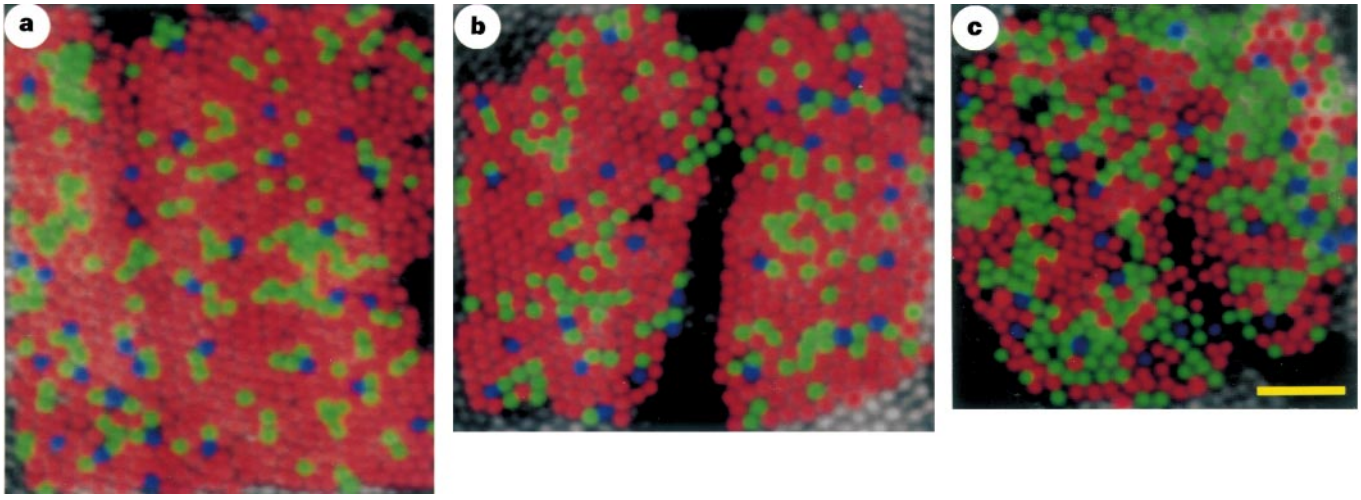

Figure 3 Pseudocolour image of the trichromatic cone mosaic. Blue, green and red colours represent the S, M and L cones, respectively. **a, b,** Subject JW's temporal and nasal retina, respectively, at one degree of eccentricity. **c,** Subject AN's nasal retina, at one degree of eccentricity. We performed a statistical test for randomness according to Diggle[27]. We compared the distribution of all intercone distances of the measured M-cone array with 100 simulations derived from the same mosaic in which the same number of M cones were randomly assigned. JW's array was no different from random at either location. AN's array showed significant clumping of the data ($P < 0.01$) but, because of optical blur, the possibility of a random assignment of M cones cannot be ruled out. Scale bar represents 5 arcmin of visual angle.

colour appearance of tiny, monochromatic light flashes[19,20] because the relative excitation of different cone classes depends on the location of the flash. A related illusion is Brewster's colours, the perception of irregular patches of pastel colour while viewing periodic black and white patterns of high spatial frequency[1,21]. Similarly, red–green isoluminant gratings with spatial frequencies above the resolution limit look like chromatic and luminant spatial noise[22]. All of these perceptual errors are examples of the aliasing produced when the three cone submosaics sample the retinal image inadequately. They are akin to the errors that occur in images taken with digital cameras that have interleaved pixels of different spectral sensitivity[1]. The clumping that results from either the random or the aggregated assignment of M and L cones exacerbates these errors.

Both of our subjects have retinal patches of 5 arcmin or more across that contain only one of the two longer-wavelength-sensitive cone classes. Although the existence of these patches indicates that the trichromat may sometimes misjudge the colour appearance of tiny objects, the patches will be beneficial in recovering high-frequency luminance patterns, because cortical neurons tuned to high spatial frequency are more likely to be fed by contiguous cones of the same class. This may explain the observation that, in some normal trichromats, there is little or no difference in resolution for gratings seen with only M cones or only L cones, or when both cone classes operate together[23]. Only when one cone class is greatly under-represented, as occurs in some heterozygous carriers for congenital X-linked protanopia, is resolution clearly mediated by the more dense submosaic[24].

The large individual differences in numbers and arrangement of cone classes that we have observed indicate that evolution has not converged on an optimum proportion of M and L cones for the human eye. Is this because red–green colour vision is a relatively new feature of vision in old-world primates[25,26], or do the statistics of natural scenes, optical blurring and clever post-receptor processing make M- and L-cone topography unimportant for visual performance? The imaging method described here allows us to address these questions, because it is now possible to assess visual performance and the circuitry of the retina in eyes for which the trichromatic mosaic is known. □

Received 16 October; accepted 26 November 1998.

1. Williams, D. R., Sekiguchi, N., Haake, W., Brainard, D. H. & Packer, O. S. in *From Pigments to Perception.* (eds Valberg, A. & Lee, B. B.) 11–22 (Plenum, New York, 1991).
2. Williams, D. R., MacLeod, D. I. A. & Hayhoe, M. Punctate sensitivity of the blue sensitive mechanism. *Vision Res.* **21,** 1357–1375 (1981).
3. Curcio, C.A. *et al.* Distribution and morphology of human cone photoreceptors stained with anti-blue opsin. *J. Comp. Neurol.* **312,** 610–624 (1991).
4. Babcock, H.W. The possibility of compensating astronomical seeing. *Publ. Astron. Soc. Pacif.* **65,** 229–236 (1953).
5. Liang, J., Williams, D. R. & Miller, D. T. Supernormal vision and high-resolution retinal imaging through adaptive optics *J. Opt. Soc. Am. A* **14,** 2884–2892 (1997).
6. Campbell, F. W. & Rushton, W. A. H. Measurement of the scotopic pigment in the living human eye. *J. Physiol. (Lond.)* **130,** 131–147 (1955).
7. Rushton, W. A. H. & Baker, H. D. Red/green sensitivity in normal vision. *Vision Res.* **4,** 75–85 (1964).
8. Pokorny, J., Smith, V. C. & Wesner, M. in *From Pigments to Perception* (eds Valberg, A. & Lee, B. B.) 23–34 (Plenum, New York, 1991).
9. Cicerone, C. M. & Nerger, J. L. The relative numbers of long-wavelength-sensitive to middle-wavelength-sensitive cones in the human fovea. *Vision Res.* **26,** 115–128 (1989).
10. Vimal, R. L. P., Pokorny, J., Smith, V. C. & Shevell, S. K. Foveal cone thresholds. *Vision Res.* **29,** 61–78 (1989).
11. Jacobs, G. H. & Neitz, J. in *Colour Vision Deficiencies* Vol. XI (ed. Drum, B.) 107–112 (Kluwer Acedemic, Netherlands, 1993).
12. Jacobs, G. H. & Deegan, J. F. Spectral sensitivity of macaque monkeys measured with ERG flicker photometry. *Vis. Neurosci.* **14,** 921–928 (1997).
13. Bowmaker, J. K. & Dartnall, H. J. A. Visual pigments of rods and cones in a human retina. *J. Physiol. (Lond.)* **298,** 501–511 (1980).
14. Dartnall, H. J. A., Bowmaker, J. K. & Mollon, J. D. Human visual pigments: microspectrophotometric results from the eyes of seven persons. *Proc. R. Soc. Lond. B* **220,** 115–130 (1983).
15. Yamaguchi, T., Motulsky, A. G. & Deeb, S. S. Visual pigment gene structure and expression in human retinae. *Hum. Mol. Genet.* **6,** 981–990 (1998).
16. Hagstrom, S. A., Neitz, J. & Neitz, M. Variation in cone populations for red-green color vision examined by analysis of mRNA. *NeuroReport* **9,** 1963–1967 (1998).
17. Mollon, J. D. & Bowmaker, J. K. The spatial arrangement of cones in the primate fovea. *Nature* **360,** 677–679 (1992).
18. Packer, O. S., Williams, D. R. & Bensinger, D. G. Photoreceptor transmittance imaging of the primate photoreceptor mosaic. *J. Neurosci.* **16,** 2251–2260 (1996).
19. Holmgren, F. Uber den Farbensinn. *Comp. Rend. Congr. Period. Intern. Sci. Med. Copenhagen* **1,** 80–98 (1884).
20. Krauskopf, J. Color appearance of small stimuli and the spatial distribution of color receptors. *J. Opt. Soc. Am.* **54,** 1171 (1964).
21. Brewster, D. On the undulations excited in the retina by the action of luminous points and lines. *Lond. Edinb. Philos. Mag. J. Sci.* **1,** 169–174 (1832).
22. Sekiguchi, N., Williams, D. R. & Brainard, D. H. Efficiency in detection of isoluminant and isochromatic interference fringes. *J. Opt. Soc. Am. A.* **10,** 2118–2133 (1993).
23. Williams, D. R. in *Advances in Photoreception*: *Proc. Symp. Frontiers Visual Sci.* 135–148 (National Academy, Washington DC, 1990).
24. Miyahara, E., Pokorny, J., Smith, V. C., Baron, R. & Baron, E. Color vision in two observers with highly biased LWS/MWS cone ratios. *Vision Res.* **38,** 601–612 (1998).
25. Nathans, J., Thomas, D. & Hogness, D. S. Molecular genetics of human colour vision: the genes encoding blue, green and red pigments. *Science* **232,** 193–202 (1986).
26. Mollon, J. D. "Tho' she kneeled in that place where they grew...": The uses and origins of primate colour vision. *J. Exp. Biol.* **146,** 21–38 (1989).
27. Diggle, P. J. *Statistical Analysis of Spatial Point Patterns* (Academic, London, 1983).

Acknowledgements. We thank D. Brainard, D. Dacey, J. Jacobs, J. Liang, D. Miller and O. Packer for their assistance. We acknowledge financial support from the Fight for Sight research division of Prevent Blindness America (to A.R.) and the National Eye Institute and Research to Prevent Blindness (to D.R.W.).

Correspondence and requests for materials should be addressed to A.R. (e-mail: aroorda@popmail.opt.uh.edu).

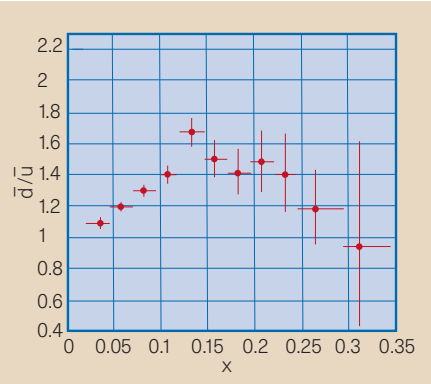

Figure 2 **The excess of down-antiquarks in the proton sea. The ratio of $\bar{d}/\bar{u}$ as a function of the fraction *x* of the momentum of the target proton carried by the struck quark, from the NuSea experiment[2].**

in puffs of hydrogen, deuterium or helium gas, which were injected into the vacuum chamber of the accelerator. As well as detecting the recoiling electron they observed the fastest meson coming out on the other side, and recorded whether it was a π^+ or a π^-. The velocity of the recoiling electron tells them the fraction *x* of the momentum of the proton or neutron that was carried by the struck quark. When *x* is large (more than about 0.2) we expect the struck quark to be a valence quark. The up and down valence quarks give particles their charge. There are two up- and one down-quarks in a proton, and two down- and one up-quarks in a neutron. Figure 1a shows the Feynman diagram for scattering off a valence up-quark in a proton, with the intermediate photon carrying momentum from the incident positron to the struck up-quark. At small *x* we also expect extra scatters, from the sea of short-lived, virtual quark–antiquark pairs produced by quantum fluctuations in the gluon field (Fig. 1b).

Simple QCD theory had predicted that this sea should contain equal numbers of up- and down-antiquarks, but the HERMES results show that there is a clear excess of down-antiquarks over the number of up-antiquarks, and the effect becomes clearer for smaller values of *x*. The NuSea experiment[2] achieved a similar result by a different method, which involved production of muon pairs in proton scattering from hydrogen and deuterium targets (Fig. 2).

Simple QCD theory does not predict an 'asymmetric sea' inside the proton; gluons should be democratic in the kinds of quark–antiquark pairs they generate. So far, the only satisfactory explanation for the excess of down- over up-antiquarks comes from more old-fashioned ideas, going back to the picture of the strong nuclear interaction that we had before QCD. Several theorists have shown that if the proton and neutron are assumed to contain virtual pions — as well as virtual quarks, antiquarks and gluons — then the asymmetry can arise quite naturally (see references in ref. 2). This does not mean that QCD is wrong, just that we still don't know how to use it to calculate all of the subtle properties of such a complicated object as a proton.□

David J. Miller is in the Department of Physics and Astronomy, University College London, Gower Street, London WC1E 6BT, UK.
e-mail: djm@hep.ucl.ac.uk

1. Ackerstaff, K. *et al.* (HERMES collaboration) *Phys. Rev. Lett.* **81,** 5519–5523 (1998).
2. Hawker, E. A. *et al.* (NuSea collaboration) *Phys. Rev. Lett.* **80,** 3715–3718 (1998).
3. Miller, G. *et al.* (SLAC–MIT collaboration) *Phys. Rev. D* **5,** 528–544 (1972).
4. Miller, D. J. *Nature* **349,** 379–387 (1991).
5. Ellis, R. K., Stirling, W. J. & Webber, B. R. *QCD and Collider Physics* (Cambridge Univ. Press, 1996).

Colour vision

A patchwork of cones

Heinz Wässle

If you look closely at the screen of a colour television, you'll see a precise mosaic of red, green and blue pixels. At a normal viewing distance, however, our eyes cannot resolve these individual pixels and, depending on their relative intensities, we perceive thousands of different colours. Television screens (and now PC monitors) are the most popular applications of the Young–Helmholtz theory of trichromacy[1], which states that human colour vision is based on three types of cone in the retina. Yet over 100 years after Helmholtz formulated his ideas, we have a paradox. Although engineers can construct perfect colour monitors, neurobiologists still do not know the details of the circuit that subserves trichromatic colour vision in humans, despite contributions from psychophysics, histology, electrophysiology, spectroscopy and molecular genetics. Now, on page 520 of this issue, Roorda and Williams[2] go some way towards addressing this problem.

Why do we not know more about human trichromacy? For one, there is no other species of animal whose retina could serve as a model. Birds, reptiles and fishes have elaborate colour vision, but their retinas differ greatly from those in primates. Many mammals have an evolutionarily ancient, dichromatic form of colour vision, but there are no known mammalian trichromates besides the primates (monkeys, apes and man)[3].

The primate retina has three types of cone, each containing a different photopigment (opsin)[4]. Their peak sensitivities lie in the violet (short wavelength S-cones), green (medium wavelength M-cones) and yellow–green (long wavelength L-cones) regions of the colour spectrum[5]. So far, only S-cones have been distinguished by microscopy and, on this basis, their circuitry has been studied in detail. As in other mammalian retinas, the S-cones make up 5–10% of all cones and form a regular mosaic. Signals from the S-cones are transmitted by special types of bipolar and ganglion cells[6,7], and there is also evidence[8] that the S-cone signal takes a separate route through the thalamus to the visual cortex.

Unfortunately L- and M-cones cannot be distinguished by their shapes or other anatomical means — their opsins differ in only 15 out of 363 amino acids, so nobody has yet succeeded in producing specific antibodies to them. But Mollon and Bowmaker[9] showed one way round this difficulty. By measuring the absorption curves of all cones in a patch of monkey retina *in vitro*, they defined the distribution of the L- and M-cones. They found equal numbers of the two cone types, randomly distributed.

Roorda and Williams[2] now take this analysis of the cone mosaic much further

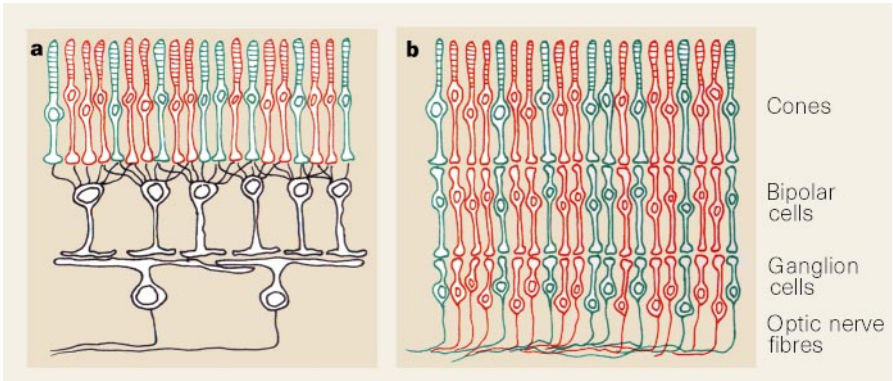

Figure 1 **Organization of the retina in different animals.** a, **In most mammalian retinas, bipolar cells pool the signals of several neighbouring cones and, in turn, ganglion cells pool the signals of several bipolar cells.** b, **In the central retina of primates, each cone is connected to a midget bipolar cell and from this to a midget ganglion cell which inherits the chromatic signal of that cone. Roorda and Williams[2] have used a new technique to show how the different types of cone are distributed in the human eye.**

and, for the first time, show the distribution of L-, M- and S-cones in the living human eye. They used an elaborate optical system ('adaptive optics') that corrects for the bad imaging quality of the cornea and lens. By differentially bleaching the retina with strong blue or red light, the authors identified L-, M- and S-cones in an extended area of retina. The proportion of L- to M-cones was nearly 4:1 in one male subject, yet closer to 1:1 in a second subject — each with normal colour vision when tested psychophysically. The L- and M-cones were randomly distributed in the two subjects, and both had large patches in which either L- or M-cones were missing.

There is no doubt that Roorda and Williams' technique, combined with psychophysical performance measurements in the same subject, will present new insights into colour vision and its variations among individuals. The patchy distribution of M- and L-cones implies that the spatial grain for colour is coarser than that for intensity, explaining why our eyes fuse the coloured pixels of the television monitor. Now we can apply this technique of imaging L- and M-cones to the monkey eye, allowing us to work out the circuitry that subserves trichromacy.

Why has trichromacy evolved in primates and not in other mammals? In most mammals, bipolar cells pool the signals of several neighbouring cones, then ganglion cells pool the signals of several converging bipolar cells (Fig. 1a). In such a highly convergent system, any chromatic information introduced into the cone mosaic by, say, a mutation that creates L- and M-cones, would be lost within the retina and would never reach the brain[10].

But the situation was different 30 million years ago for primates. During evolution, the primate eye and retina have been optimized for the highest spatial resolution. This required a high density of cones and a low ratio of cones to ganglion cells in the 'acuity pathway'. The anatomical limits for this optimization were reached when each cone was connected, through a midget bipolar cell, to a midget ganglion cell (Fig. 1b). In this way, a 'private line' to the brain was established. Only after evolution of this one-to-one connection in the central retina did a subsequent mutation create the patchy distributions of L- and M-cones at random locations[11]. The one-to-one midget-cell system of the central retina could then transmit this chromatic information to the brain. Gradually, the selective advantage of trichromatic vision must have led the colour-processing pathways to proliferate in cortical, and perhaps even subcortical, centres. The well-known plasticity of the brain could easily have allowed such changes. The idea that trichromacy piggybacks on the high-acuity system also indicates that the midget ganglion cells do a double duty in visual signalling — an idea that has been promoted for some years[12]. □

Heinz Wässle is at the Max Planck Institut für Hirnforschung, Deutschordenstrasse 46, D-60528 Frankfurt/Main, Germany.
e-mail: waessle@mpih-frankfurt.mpg.de

1. von Helmholtz, H. *Treatise on Physiological Optics* (ed. Southall, J. P.) 3 Vols (Dover, New York, 1962).
2. Roorda, A. & Williams, D. R. *Nature* **397,** 520–522 (1999).
3. Jacobs, G. H. *Biol. Rev.* **68,** 413–471 (1993).
4. Nathans, J., Merbs, S. L., Sung, C. H., Weitz, C. J. & Wang, J. *Annu. Rev. Genet.* **26,** 403–424 (1992).
5. Schnapf, J. L., Kraft, T. W. & Baylor, D. A. *Nature* **325,** 439–441 (1987).
6. Kouyama, N. & Marshak, D. W. *J. Neurosci.* **12,** 1233–1252 (1992).
7. Dacey, D. M. & Lee, B. B. *Nature* **367,** 731–735 (1994).
8. Martin, P. R., White, A. J. R., Goodchild, A. K., Wilder, H. D. & Sefton, A. E. *Eur. J. Neurosci.* **9,** 1536–1541 (1997).
9. Mollon, J. D. & Bowmaker, J. K. *Nature* **360,** 677–679 (1992).
10. Wässle, H. & Boycott, B. B. *Physiol. Rev.* **71,** 447–480 (1991).
11. Mollon, J. D. *J. Exp. Biol.* **146,** 21–38 (1989).
12. Ingling, C. R. Jr & Martinez-Uriegas, E. *Vision Res.* **23,** 1495–1500 (1983).

Oceanography

Bacteria and silica cycling

Victor Smetacek

As a graduate student who enjoyed counting plankton under the microscope, I felt frustrated when confronted with an occasional sample that contained almost nothing except a few bacteria flitting or gliding about on the slide. The bacteria were apparently responsible for the barrenness of the slide, and had thrived because the sample had escaped its shot of preservative. Mysteriously, the silica shells of the diatoms had also vanished, although they were beautifully preserved in the treated samples. The observation contradicted the view that diatom shells are of no nutritional value and that their dissolution is controlled by physico-chemical and not biological factors.

This dogma has now itself been dissolved (and hence my hunch borne out) by the elegant study by Bidle and Azam on page 508 of this issue[1]. They show that bacteria do indeed 'gnaw' enzymatically into diatom shells, thereby hastening their dissolution rates significantly (Fig. 1). The authors also show that adding proteases (enzymes that break down proteins) had the same effect as live bacteria, indicating that a protein coating provides protection from dissolution.

Diatoms dominate phytoplankton blooms in the ocean, so the finding adds to our growing understanding of how planetary elemental cycles are geared to each other. In the emerging view, wind-blown dust from the continents increases ocean productivity by providing iron[2], which is often a limiting element. In large areas of the open ocean — the high-nutrient, low-chlorophyll (HNLC) regions — iron deficiency constrains growth rates not only of phytoplankton[2] but also of bacteria[3]. In some regions, silicic acid (dissolved silica) is in short supply relative to the major nutrients nitrate and phosphate[4]. For instance the N:P ratio across the Southern Ocean varies by less than 10% but the Si:N ratio ranges from 0.15 in the north to 3 in the south. Because diatom demand for Si:N is about 1, the discrepancy in dissolved nutrient ratios indicates that nitrogen is recycled more efficiently within the surface layer than silica. Hence the finding that microbial breakdown of protein also enhances silica dissolution[1] has interesting implications, because until now diatoms have been thought to protect their surface by secreting mucus (carbohydrates).

The world ocean is strongly undersaturated in silicic acid but its cycle is in steady state, with the annual input from rivers — about six tera (10^{12}) moles — being balanced by burial of diatom shells in sediments[5]. However, the sediments underlying the productive ocean

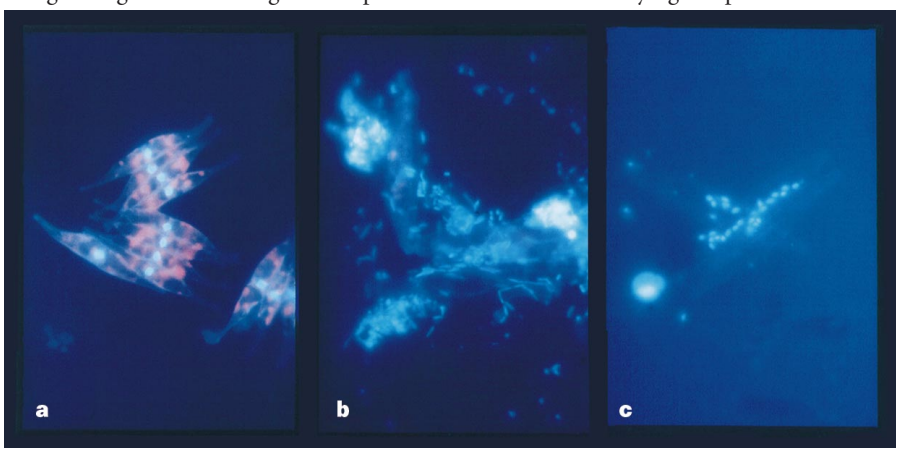

Figure 1 **The case of the disappearing diatoms — an example of Bidle and Azam's experiments[1]. These pictures are a time series, running left to right, showing bacterial attack on the silica shells of the diatom *Cylindrotheca fusiformis*. In** a, **time zero, the diatoms' integrity is intact.** b **and** c **show their progressive dissolution after two and seven days, the bacteria staining bright blue. (Courtesy F. Azam.)**